

Mechanochromic Photonic Gels

Edwin P. Chan,* Joseph J. Walsh, Augustine M. Urbas, and Edwin L. Thomas*

Polymer gels are remarkable materials with physical structures that can adapt significantly and quite rapidly with changes in the local environment, such as temperature, light intensity, electrochemistry, and mechanical force. An interesting phenomenon observed in certain polymer gel systems is mechanochromism – a change in color due to a mechanical deformation. Mechanochromic photonic gels are periodically structured gels engineered with a photonic stopband that can be tuned by mechanical forces to reflect specific colors. These materials have potential as mechanochromic sensors because both the mechanical and optical properties are highly tailorable via incorporation of diluents, solvents, nanoparticles, or polymers, or the application of stimuli such as temperature, pH, or electric or strain fields. Recent advances in photonic gels that display strain-dependent optical properties are discussed. In particular, this discussion focuses primarily on polymer-based photonic gels that are directly or indirectly fabricated via self-assembly, as these materials are promising soft material platforms for scalable mechanochromic sensors.

called bandgaps or stopbands reflect light incident from outside the material at these frequencies and angles (Figure 1). Examples of such materials occur in nature, such as the morpho butterfly and opals.^[1–3] Artificial photonic crystals can also be fabricated out of ceramics, metals, polymers, and in particular, semiconductors. Their ability to interact and control light propagation render them useful in many optical-based devices including low-loss mirrors^[4,5] and lasers,^[6] color-changing paints and inks, chemical^[7–10] and mechanical^[11–26] sensors, and displays,^[27–29] as well as in optical fiber devices for telecommunications^[30] and medicine.^[31,32]

The phenomenon that produces interference color in a photonic crystal is analogous to the electronic bandgap present in semiconductors. In this case, the color is due to the presence of a photonic bandgap, or stopband, that arises because of the periodic dielectric function of the material and prevents photons of a certain frequency from propagating, in much the same way that electrons of certain energy cannot propagate in the ionic lattice of semiconductors.^[33] Determining the photonic band structure of a photonic crystal involves principles of solid-state physics and electromagnetism, and is not the focus of this contribution. A basic understanding of band structures can be gained by considering the multilayer or 1D periodic system, which consists of an arrangement of layered materials with different dielectric constants or refractive indices periodic along only one direction (Figure 1). The simplest case of this material system is for a pair of layers of thickness d_1 and d_2 with isotropic refractive indices n_1 and n_2 . Such a material is commonly referred to as a Bragg reflector and the stopband arises from constructive and destructive interference reflections at each material interface. Specifically, incident light is partially reflected at the interfaces created by the two materials having different indices and the sum contribution of reflection from the layers leads to constructive interference of some wavelength of light. The largest bandgap for propagation along the direction of periodicity occurs for a quarter-wave stack where each layer has an optical thickness, the product of the refractive index and the physical thickness ($= n \cdot d$), equal to 1/4th of the incident wavelength. In order to generate a stopband for a wavelength of around 600 nm, the optical thickness for each material layer must be 150 nm. For example, a polymeric material with a typical refractive index $n \approx 1.5$ would require layer thickness of $d \approx 100$ nm. For a 1D photonic crystal consisting of two materials, the center wavelength of the stopband (λ) based on the quarter-wave condition can be simply written as:

1. Introduction

Photonic crystals derive their selective reflection from photonic bandgaps, which develop due to a periodic arrangement of materials having different dielectric constants. The specific spatial arrangement of the dielectric materials along one or more principal axes in one-, two-, and three-dimensional (1D, 2D, and 3D) periodic structures gives rise to frequency bands and propagation directions that are characterized by evanescent modes. These so

periodic dielectric function of the material and prevents photons of a certain frequency from propagating, in much the same way that electrons of certain energy cannot propagate in the ionic lattice of semiconductors.^[33] Determining the photonic band structure of a photonic crystal involves principles of solid-state physics and electromagnetism, and is not the focus of this contribution. A basic understanding of band structures can be gained by considering the multilayer or 1D periodic system, which consists of an arrangement of layered materials with different dielectric constants or refractive indices periodic along only one direction (Figure 1). The simplest case of this material system is for a pair of layers of thickness d_1 and d_2 with isotropic refractive indices n_1 and n_2 . Such a material is commonly referred to as a Bragg reflector and the stopband arises from constructive and destructive interference reflections at each material interface. Specifically, incident light is partially reflected at the interfaces created by the two materials having different indices and the sum contribution of reflection from the layers leads to constructive interference of some wavelength of light. The largest bandgap for propagation along the direction of periodicity occurs for a quarter-wave stack where each layer has an optical thickness, the product of the refractive index and the physical thickness ($= n \cdot d$), equal to 1/4th of the incident wavelength. In order to generate a stopband for a wavelength of around 600 nm, the optical thickness for each material layer must be 150 nm. For example, a polymeric material with a typical refractive index $n \approx 1.5$ would require layer thickness of $d \approx 100$ nm. For a 1D photonic crystal consisting of two materials, the center wavelength of the stopband (λ) based on the quarter-wave condition can be simply written as:

Dr. E. P. Chan
Materials Science and Engineering Division
National Institute of Standards and Technology
100 Bureau Drive, MS 8542, Gaithersburg,
MD 20899, USA
E-mail: edwin.chan@nist.gov



Dr. J. J. Walsh
Department of Materials Science and Engineering
Massachusetts Institute of Technology
Rm 6-113, 77 Massachusetts Avenue, Cambridge, MA 02139, USA

Dr. A. M. Urbas
Air Force Research Laboratory
Materials and Manufacturing Directorate
Wright-Patterson Air Force Base, Ohio 45433, USA

Prof. E. L. Thomas
Dean of Engineering
Department of Mechanical Engineering and Materials Science
Rice University
P.O. Box 1892, Houston, TX 77251, USA
E-mail: elt@rice.edu

DOI: 10.1002/adma.201300692

$$\lambda = 2(n_1d_1 + n_2d_2) \quad (1)$$

Looking at Equation 1, it is clear that the stopband can be tuned by changing the optical path length for either layer, by changing the thickness or refractive index or both.

While Bragg reflectors have been studied for over 100 years, their application as mechanochromic sensors has only been explored in any depth over the last decade.^[11–26] A primary reason for the limited research is attributed to the fact that traditional photonic crystals fabricated from “hard materials” have too limited a range of optical and mechanical properties necessary for mechanochromic sensing. Since the mechanical properties of most traditional photonic crystals are only elastic up to a few percent strain, the corresponding stopband shift with strain ($\Delta\lambda = \lambda_0 \cdot \Delta\epsilon$) would be small and difficult to detect without high-precision instrumentation. For practical application of a photonic crystal as a mechanochromic sensor, the stopband shift with mechanical deformation must be sufficiently large to enable simple (even just by eye) optical detection.

Compared with their inorganic counterparts, polymer-based photonic crystals, particularly polymer gels, provide more potential as mechanochromic sensors because of their extreme elasticity. Traditionally, polymer gels are physically- or chemically-crosslinked polymer networks swollen with a significant amount of low-molar mass solvents. However, swelling with other diluents, such as ionic liquids, plasticizers, polymers, as well as nanoparticles, provides a large parameter space to tailor both the optical and mechanical properties of polymer-based photonic crystals, which we refer to as photonic gels.

We begin with an overview of polymer-based photonic crystals that exhibit mechanochromic properties to familiarize the reader with developments in the field. Next, we discuss photonic gels and the individual developments related to mechanochromic sensing. In particular, we present simple relationships that describe the change in color with applied stress or strain. Finally, we end with a brief discussion on the future directions for mechanochromic sensing.

2. Polymer-Based Photonic Crystals for Mechanochromic Sensing

An effective mechanochromic sensor requires that the information pertaining to local stress and strain be encoded in the optical response of the material and is sufficiently large to enable optical detection. To describe this requirement, we

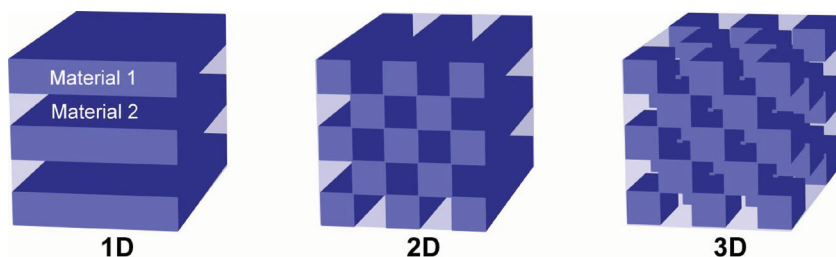


Figure 1. Schematic representation of 1D, 2D, and 3D photonic crystals. The classification of dimensionality is determined by the spatial arrangement of the two materials having different dielectric constants.



Edwin P. Chan is a staff scientist in the Materials Science and Engineering Division at the National Institute of Standards and Technology (NIST). He received a B.S. in Materials Science & Engineering from the Pennsylvania State University in 2000, an M.S. in Materials Science & Engineering from the Massachusetts Institute

of Technology in 2003, and a Ph.D. in Polymers Science and Engineering from the University of Massachusetts Amherst in 2007. His current research focuses on the structure, transport, and mechanics of polymer gels and networks.



Edwin L. “Ned” Thomas is the William and Stephanie Sick Dean of the George R. Brown School of Engineering at Rice University, where he holds joint appointments in the Departments of Mechanical Engineering and Materials Science and Chemical and Biomolecular Engineering. He received a B.S. in Mechanical

Engineering from the University of Massachusetts Amherst in 1969 and a Ph.D. in Materials Science and Engineering from Cornell University in 1974. Thomas was head of the Department of Materials Science and Engineering at the Massachusetts Institute of Technology from 2006–2011. His research is currently focused on using 2D and 3D lithography, direct-write and self-assembly techniques for creating metamaterials with unprecedented mechanical and thermal properties.

define the mechanochromic sensitivity, $\Delta\lambda/\Delta\epsilon$, which defines the shift in the stopband wavelength with the incremental change in applied strain. **Table 1** summarizes the mechanochromic sensitivity of polymer-based photonic crystals.

As the table indicates, the mechanochromic sensitivity is highly dependent on the specific material system, with sensitivity values ranging from $\Delta\lambda/\Delta\epsilon \approx 0.7$ to 5.3. This broad range in mechanochromic sensitivity is strongly connected with the mechanical

Table 1. Summary of the mechanochromic properties of polymer-based photonic crystals

Material	Mechanochromic sensitivity, $\Delta\lambda/\Delta\varepsilon$ [nm/%]	Stopband peak range, λ [nm]	Maximum percent strain, ε
Co-extruded polymer multilayers (1D) ^[34]	1.85	565 to 750	100% uniaxial tension
Co-extruded polymer multilayers (1D) ^[35]	1.52	410 to 600	125% uniaxial tension
Concentric polymer multilayers (1D) ^[36]	2.08	550 to 800	120% uniaxial tension
Cholesteric liquid crystals (1D) ^[15]	1.41	544 to 630	61% equi-biaxial tension
Polymer dispersed liquid crystals (1D) ^[37]	2.86	590 to 713	43% uniaxial compression
Anisotropic hydrogel lamellar copolymer(1D) ^[23]	2.89	415 to 600	64% uniaxial compression
Anisotropic hydrogel lamellar copolymer(1D) ^[38]	0.65	350 to 610	400% uniaxial tension
Block copolymer (PS- <i>b</i> -PI, 1D) ^[39,40]	1.48	562 to 642	50% uniaxial compression
Block copolymer gel (PS- <i>b</i> -sP2VP, 1D) ^[26]	4.80	520 to 760	30% uniaxial compression
Synthetic opal elastomer (PDMS backfilled, 3D) ^[18]	1.50	560 to 590	20% uniaxial tension
Synthetic opal elastomer (Acrylate backfilled, 3D) ^[16]	5.25	466 to 550	16% uniaxial compression and tension
Synthetic opal elastomer (Hydrogel backfilled, 3D) ^[13]	3.67	525 to 580	15% uniaxial compression

behavior of the materials system subject to different deformation modes. Additionally, only 1D and 3D photonic crystals are commonly used in mechanochromic sensing. This trend is associated with ease and practicality of fabrication and application. In the next section, we will discuss the structures and mechanisms that contribute to the mechanochromic.

2.1. Materials Systems

2.1.1. 1D Photonic Crystals

As we have already discussed, a 1D photonic crystal (Figure 1) possesses a stopband perpendicular to the layers, thus making it an ideal geometry for mechanochromic sensing applications since the photonic color can be easily viewed normal to a surface. Both top-down and bottom-up fabrication strategies have been employed for constructing polymer-based 1D photonic crystals. A commercially relevant top-down approach is the coextrusion approach of multilayer polymer films. Developed during the late 1960s by Dow Chemical, these multilayers consist of two or more different polymers coextruded together to form a dielectric mirror.^[41] This continuous film-coextrusion

process utilizes multiple layer-multiplying die elements to form films effectively consisting of hundreds to thousands of alternating polymer layers. For a multilayer of A and B homopolymers, the two molten polymers are combined through a feedblock to form an ABA trilayer; this trilayer is then split vertically at the layer-multiplying die element, then spread horizontally and recombined.^[42] Currently, 3M produces similar coextruded films that are commercially available. Wideband filters (e.g., mirrors) are also available from 3M and are films made from polymer layers with graded thickness and high birefringence.^[43,44] The Baer group has extended this coextrusion method to fabricate elastomeric photonic crystals.^[34,35] The stopband can be tuned by the thickness of the layers and the stopband intensity can be adjusted by a number of alternating polymer layers, both of which can be controlled via the coextrusion process. When deformed, these elastomeric multilayers change color. This fabrication strategy is highly scalable and amenable to a variety of polymer combinations, which is very promising for mechanochromic sensing applications since elastomeric polymers are highly deformable materials, and their mechanical properties can be tuned based on a judicious choice of polymers with specific mechanical and optical properties. More recently, Kolle et al. used a conceptually similar layer multiplying approach to generate a concentric 1D photonic bandgap fiber by rolling a bilayer film consisting of two different elastomers around a thin glass-fiber core to form the multilayer cladding with a stopband that is strain-sensitive.^[36]

A bottom-up analog to these coextruded polymer multilayers is the lamellar phase of block copolymers (BCPs). Unlike polymer multilayers, which require energy-intensive melt-processing and are limited to an alternating layered nanostructure, BCPs self-assemble into a variety of periodic block microdomains whose morphology and structural length-scale are governed by the thermodynamics of microphase separation. The molecular architecture of each polymer and degree of immiscibility between the polymer blocks determine the final morphology. Because the morphology forms spontaneously, conformal, curved and topographically complex coatings can be made. Additionally, different mechanical properties can be imparted into the BCPs by a judicious choice of polymer for each of the blocks.

For a diblock copolymer composed of covalently bonded blocks of homopolymers A and B, several morphologies, including body-centered cubic, cylindrical, bicontinuous cubic, and lamellar, can be obtained depending on the relative composition or volume fraction (Figure 2). The size of an individual BCP microdomain scales with the molecular mass or total number of monomer repeat units (N) of the corresponding polymer. For a diblock BCP that forms lamellar morphology, the size of the microdomain scales as $N^{2/3}$.^[45] Besides having a refractive-index contrast between the respective block domains, a BCP photonic crystal with a stopband in the visible wavelengths requires that each homopolymer has a sufficiently large number of monomer repeats to create the necessary 100 nm domain thickness; in other words, the total molecular molar mass is about 10^6 g mol⁻¹.^[46,47]

Since one of the key requirements of a photonic crystal is a periodic variation in the refractive index, materials with anisotropic refractive indices can also be candidate materials.

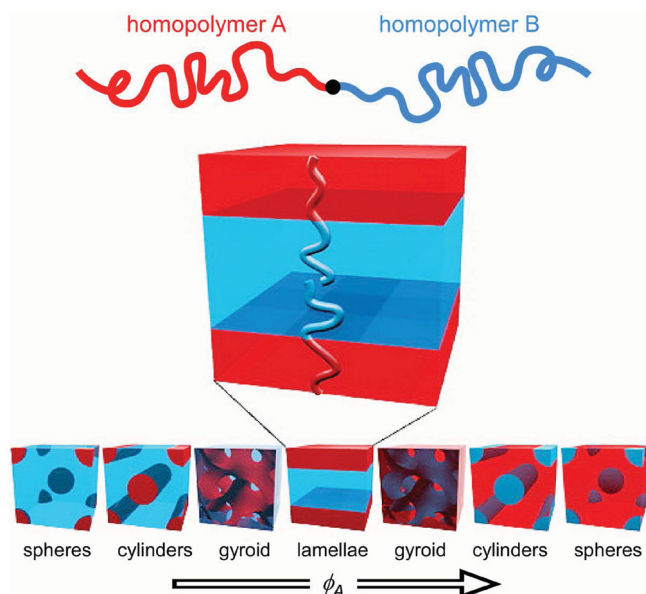


Figure 2. Block copolymer phase diagram for an AB linear diblock. Reproduced with permission.^[48] Copyright 2007, Elsevier.

The coextruded film by 3M is one example of such a material where the anisotropic refractive indices develop due to shearing of the layers during coextrusion. Another example is liquid-crystalline materials (LCs), which consist of mesogens that are small, rigid-rod- or disk-like molecules. Twisted-nematic liquid crystals (TNLCs) have been used for decades in display technology since the mesogens can be reoriented with an applied electric field, which leads to large changes in the optical-transmission properties of the material. Side-chain liquid-crystalline block copolymers have been developed to display temperature- and electric-field-tunable photonic bandgaps. Specifically, Osuji and co-workers used hydrogen bonding to link small-molecule mesogens to a coil-coil diblock copolymer, to form a liquid-crystalline phase in one of the block domains,^[49,50] thus resulting in a photonic-bandgap material whose refractive index is tunable with external stimuli.^[50]

Besides electric and magnetic fields, the orientation of the mesogens can also be changed via a mechanical stress field. This effect can be easily observed when one touches an LC-based flat-panel display, which is due to re-orientation of the mesogens due to mechanical compression normal to the display surface. Cholesteric liquid crystals (CLCs) contain mesogens that are chiral in nature. Thus, these materials have a rotation of the molecular alignment through the material thickness, which is described as a pitch. This twist of the molecular orientation also creates a periodic variation in dielectric properties, which gives rise to selective reflection of one circular polarization based on Bragg reflection.^[51] Additionally, CLCs have been engineered as elastomers that can change color in response to mechanical deformation, making them candidate materials for tunable optical filters or reflectors.^[37,52–55] The tunability and reversibility of these CLC elastomers comes about because of the change in pitch with applied stress and the entropic elastic restoring force from the deformed crosslinked network and

director field. The pitch of a CLC is sensitive to the chemical composition of the system, as well as temperature, making a wide parameter space available for changing the photonic properties of these materials. Similar to BCPs, CLC elastomers are quite scalable due to their ability to self-assemble into functional nanostructures over large areas and then be crosslinked.

Another promising self-assembled system that displays mechanochromic behavior is the anisotropic hydrogel developed by Haque et al. These hydrogels are 1D photonic crystals whose photonic structure is defined by the assembly of hydrophobic poly(dodecyl glyceryl itaconate) (PDGI) bilayers embedded in a polyacrylamide matrix.^[23,38] Unlike typical hydrogels that have rather poor mechanical properties, this anisotropic hydrogel is very tough and can support >2000% strain before failure. This enhanced toughness is attributed to the non-covalent hydrophobic association of the PDGI bilayers serving as sacrificial bonds to provide significant energy dissipation during mechanical deformation.^[38] Strain-to-failure ratios of this magnitude are sometimes found in nature but rarely in mechanochromic polymers.

2.1.2. 3D Photonic Crystals

Self-assembled structures have also been used as scaffolds or templates for producing 3D mechanochromic materials. These templates include face-centered cubic structures of spheres (synthetic opals) produced by self-assembly of polystyrene or silica colloids, which are then subsequently infiltrated with elastomeric^[18] or gel^[19,20,56–58] precursors and then crosslinking to ensure reversible mechanochromism. The colloidal template can be removed by dissolution of the particles while preserving the soft matrix to obtain the inverse face-centered-cubic structure. Removal of the colloids not only enhances the refractive-index contrast of the mechanochromic material, because they are now replaced with air, but also changes its mechanical properties.

Another candidate 3D photonic material is a polystyrene-block-polyisoprene, forming the double-gyroid phase.^[59] It consists of two 3D-bicontinuous polystyrene networks in a polyisoprene continuous matrix. Similarly, etching of the polyisoprene matrix with ultraviolet light yields a polystyrene scaffold with an enhanced refractive-index contrast, since the polyisoprene is now replaced with air. Alternatively, this bicontinuous structure can be used as a template by infiltration with a gel precursor followed by dissolution of the polystyrene scaffold to tune both the optical and mechanical properties.

2.2. Mechanochromism of Photonic Crystals

Mechanochromism in a photonic crystal is based on stopband shifts due to changes in the optical path length of one or more of the domains. This change corresponds to the form, magnitude, and temporal characteristics of the applied deformation. For example, consider a 1D photonic crystal under the three basic modes of compression, tension, and shear (Figure 3a). For simplicity, we consider that this photonic crystal consists of two materials with different refractive indices (n_1 , n_2) but similar thicknesses ($d_1 \approx d_2$) and moduli ($E_1 \approx E_2$), possesses

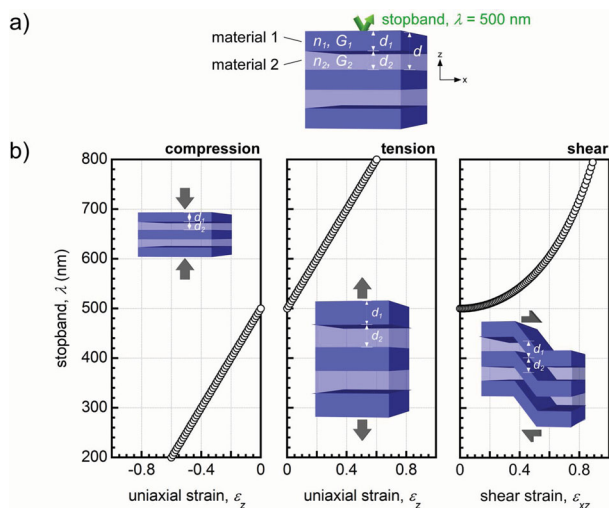


Figure 3. General deformation modes resulting in stopband changes of a 1D photonic crystal viewed at normal incidence. a) Example of a 1D photonic crystal consisting of two materials with different refractive indices (n_1, n_2) but similar layer thicknesses ($d_1 \approx d_2$) and elastic moduli ($E_1 \approx E_2$). b) Stopband changes as a function of applied strain. Left: The stopband shifts to shorter wavelengths linearly with compressive strain (ϵ_z) due to a reduction in optical path length. Center: The stopband shifts to longer wavelengths linearly with tensile strain (ϵ_z) due to an increase in optical path length. Right: The stopband shifts to longer wavelengths non-linearly when the shear strain (ϵ_{xz}) induces changes in lamellar orientation, leading to changes in the layer spacing. In all three deformation modes, we assumed that the refractive indices are strain-independent: thus, the optical path length changes are due to changes in layer thicknesses and reorientation.

strain-independent refractive indices, and behaves mechanically as a linear-elastic material. Regardless of the specific mode, the applied deformation either deforms or distorts this layered structure to cause an alteration in layer dimensions and/or refractive index, which changes the optical path length for each layer, thus resulting in a stopband shift. However, the specific change in the optical path length is unique to each deformation, which implies a unique relationship between the stopband position and the strain (ϵ) (Figure 3b).

Uniaxial compression and tension applied along the normal to the layer thickness are similar, in that they can be explained in terms of a decrease or an increase in the layer thicknesses, respectively. Based on Equation 1, the stopband vs. strain relationship is defined as:

$$\lambda(\epsilon_z) = 2n_1d_1 \cdot (1 + \epsilon_{z,1}) + 2n_2d_2 \cdot (1 + \epsilon_{z,2}) \quad (2)$$

$$\epsilon_z = \phi_1\epsilon_{z,1} + \phi_2\epsilon_{z,2} \quad (3)$$

Equation 3 is obtained from the classical Reuss composite model with the volume fractions of materials 1 and 2 defined as $\phi_1 = \frac{d_1}{d}$ and $\phi_2 = \frac{d_2}{d}$, respectively. For our 1D photonic crystal, where materials 1 and 2 have similar modulus and thickness, Equation 2 simplifies to $\lambda(\epsilon_z) = (2n_1d_1 + 2n_2d_2) \cdot (1 + \epsilon_z)$.

Shear is unique in that it involves a shape change as opposed to a volume change. This leads to a rotation of the layers, plus a translation, which causes an effective change in the optical path

length along the original viewing direction (Figure 3c). Therefore, the stopband increases non-linearly with shear strain (ϵ_{xz}), and the relationship for our symmetric 1D photonic crystal is:

$$\lambda(\epsilon_{xz}) = \frac{2(n_1d_1 + n_2d_2)}{\cos(\tan^{-1}(\epsilon_{xz}))} \quad (4)$$

3. Mechanochromism of Photonic Gels

As Table 1 shows, photonic gels have significantly higher mechanochromic sensitivity values, making them ideal candidates as simple visual mechanochromic sensors. Compared with traditional polymer gels, photonic gels consist of periodic dielectric structures on the mesoscale. Furthermore, this periodic structure and refractive-index contrast must be maintained to be functional as mechanochromic sensors. Therefore, only a few material systems have been shown to exhibit these properties. While there are several strategies to construct photonic gels, we limit our discussion primarily to BCP-based systems, because this material platform offers a vast parameter space in tuning both the optical and mechanical properties. We will briefly discuss colloidal-based photonic gels since there are currently no 3D BCP-based photonic gels. For a given BCP, we can select the constituent polymers, add homopolymer, diluent, or solvent to generate a range of morphologies and domain spacings by selectively swelling one or both of the microdomains, while at the same time adjusting the mechanical response to suit a particular sensing application. Swelling can significantly increase the dimensions of the microdomains reducing the need for high-molecular-mass BCPs, which are often challenging to synthesize and process into defect-free films.

Almost all polymers have the propensity to swell with the appropriate solvent or swelling agent. Depending on the chemical affinity of the polymer to the swelling agent, the extent of swelling can span from $\approx 10\%$ to over $\approx 1000\%$, which enables the generation of a photonic gel using a BCP of moderate molecular mass ($M_n \approx 10^5 \text{ g mol}^{-1}$). An early demonstration of this swelling approach was the incorporation of low-molecular-mass homopolymers into a diblock copolymer of polystyrene-*block*-polyisoprene (PS-*b*-PI).^[60] In this study, homopolymers of PS and PI ($M_{n,PS} = M_{n,PI} = 13\,000 \text{ g mol}^{-1}$) were systemically blended into a nearly symmetric PS-*b*-PI of moderate molecular mass ($M_{n,PS}/M_{n,PI} = 194\,000 \text{ g mol}^{-1}/197\,000 \text{ g mol}^{-1}$). Specifically, this blending leads to stopband shifts toward longer visible wavelengths, due to swelling of the microdomains to larger layer thicknesses, which increase with the volume fractions of the two homopolymers incorporated into the BCP blend.

Besides tuning the photonic stopband by adding low-molar-mass homopolymers to swell the BCP microdomains, nanoparticles have also been used to modify the dielectric properties of a BCP photonic crystal.^[61] Specifically, polystyrene-functionalized gold nanoparticles were blended into a nearly symmetric diblock copolymer of polystyrene-*block*-polyethylene/propylene (PS-*b*-PEP) ($M_{n,PS}/M_{n,PEP} = 400\,000 \text{ g mol}^{-1}/400\,000 \text{ g mol}^{-1}$) that formed the lamellar morphology. Due to the PS ligands, the nanoparticles sequestered to the PS microdomains. This resulted in a stopband shift to a slightly longer wavelength due to an enhancement in the refractive index of the PS microdomain, as well as

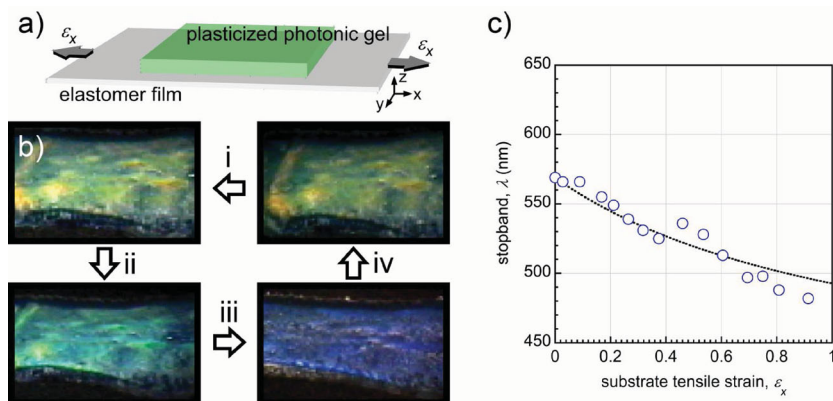


Figure 4. Mechanochromism of the plasticized PS-*b*-PI photonic gel. a) The gel is deformed indirectly by stretching the elastomeric supporting film. b) Optical micrographs of the deformed gel. The color shifts from green to blue during deformation and, when the deformation is relaxed, the green color is recovered. The cycle is represented by the arrows: the yellow-green sample is stretched in (i) to a green color; further stretching in (ii) yields a blue-green sample; continued stretching in (iii) results in a color change to blue, which represents the shortest spacing of the observed colors; and finally, relaxation in (iv) recovers the initial color of the sample. The cycle shown can be repeated with consistent performance. c) The peak reflective wavelength is plotted as a function of the measured deformation of the elastomer film, which is represented as tensile strain. The stopband shifts to shorter values as the sample is stretched in accordance with the observed color change. The solid curve represents the scaling relationship defined by Equation 2. Reproduced with permission.^[62] Copyright 2003, Massachusetts Institute of Technology.

the refractive-index contrast, without significant changes to the microdomain size. These approaches provide a flavor of the strategies in tuning either the layer thickness or refractive index of the BCP photonic crystals. In the next section, we discuss the application of these strategies in the context of BCP photonic gels. We focus primarily on systems that have been demonstrated as mechanochromic sensors and discuss their particular operating mechanism.

3.1. Block Copolymer Photonic Gel Systems

3.1.1. Plasticized BCP Photonic Gels

Swelling with a solvent represents one of the simplest and most versatile routes to enhancing the physical, optical, and mechanical properties of a polymer network. However, most solvents are volatile, which causes an unstable change in the polymer properties unless the overall system is sealed. To circumvent this issue, Urbas and co-workers used dioctyl-phthalate (DOP), a common non-volatile plasticizing agent for polymers, to swell a nearly symmetric diblock of PS-*b*-PI.^[62] Both the PS and PI microdomains swell significantly since DOP is a neutral solvent for both polymers, resulting in a photonic gel that is also viscoelastic, and hence hysteretic, since the glassy PS is now plasticized.

This plasticized BCP photonic gel is responsive to various mechanical deformations, including uniaxial tension, peel, and shear. Under uniaxial tension, quantifying local deformation by monitoring the stopband shift is straightforward (Figure 4).^[62] The color change as a function of deformation of this gel can be measured directly by coating it onto an elastomeric substrate

followed by stretching (Figure 4a). Figure 4b shows a series of optical micrographs of the deformation cycle of the plasticized photonic gel, the deformation cycle, and the associated color change.

To quantify the local deformation of this gel, the stopband shift versus deformation was measured using spectral measurements. As shown in Figure 4c, the stopband shifts to lower wavelength with stretching quantified as tensile strain, ϵ_x . On the polymer level, this uniaxial tensile strain compresses the plasticized BCP microdomains that are oriented parallel to the elastomer film surface, thus leading to the stopband shift.

Because the entire BCP is uniformly swollen with the plasticizer, this material can be described as a highly solvated polymer network consisting of physical entanglements. Therefore, the microdomain dimension and shear modulus of both layers are $d_1 \approx d_2$, and $G_1 \approx G_2$. This assumption enables the application of classical mechanical deformation models for polymer gels, which links deformation on the macroscopic level to the polymer-chain level.^[63] Specifically, we apply the junction-affine polymer network model to describe the mechanical response. This model deviates from the affine network model in that it considers the local response of the polymer network to be slightly different from the macroscopic deformation. Specifically, the local deformation of the BCP microdomains oriented parallel to the film surface, α_z , is related to the macroscopic tensile strain ϵ_x : $(\alpha_z)^2 = (2 + \epsilon_x)/(2(1 + \epsilon_x))$. The strain-dependent stopband change is defined as:

$$\lambda(\epsilon_x) = (2(n_{sPS}d_{sPS} + n_{sPI}d_{sPI})) \cdot \left(\frac{2 + \epsilon_x}{2(1 + \epsilon_x)} \right)^{1/2} \quad (5)$$

The parameters n_{sPS} , n_{sPI} and d_{sPS} , d_{sPI} correspond to the refractive index and layer thickness of the swollen PS and PI microdomains, respectively. As shown by the fit in Figure 4c, Equation 5 provides good agreement with the experimental results. While morphological characterization is needed to understand the local deformation of the BCP microdomains, the results demonstrate that this plasticized BCP approach provides an indicator of deformation that can be easily visualized with the naked eye.

Besides mechanochromic sensing of uniaxial deformation, this plasticized BCP photonic gel can also measure the stress distribution during a peel experiment (Figure 5).^[62] In this experiment, a small amount of the same BCP and plasticizer mixture was placed between a glass substrate and a clear plastic film. After equilibration to obtain a highly colored and reflective material, the clear plastic film was peeled back from the glass substrate, deforming the plasticized BCP gel (Figure 5a). As shown in Figure 5b, this deformation caused a color change at the separation edge (i.e., the peel front). Since the undeformed gel is violet in color, the shift to a longer wavelength at the peel front

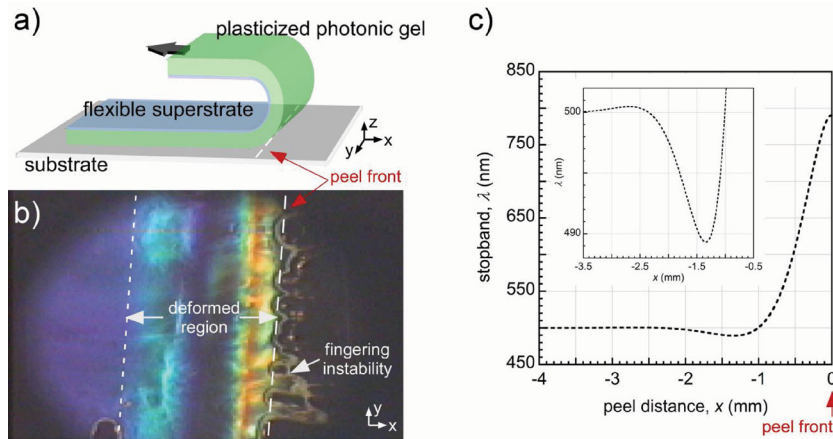


Figure 5. Peeling of a plasticized BCP photonic gel. a) The gel layer, which is sandwiched between a rigid substrate and a flexible superstrate, is peeled away from the substrate to cause development of a peel front. b) Optical micrograph of the peel experiment showing the mechanochromic response of the gel as it is peeled from the right to left. Ahead of the peel front, the gel develops Saffman–Taylor-like fingering instability to relieve the maximum stress. Significant stopband shifts occur locally and directly behind the peel front, which is indicative of the strain field imposed by the peel process. The undeformed gel has a violet color but changes to predominately longer wavelengths closer to the peel front where the strain is the highest. Part (b) reproduced with permission.^[62] Copyright 2003, Massachusetts Institute of Technology. c) Predicted stopband change as a function of the distance away from the peel front, demonstrating the intricate change in the stopband position. The inset is a magnification of the plot illustrating the alternating tensile and compressive regions of the gel behind the peel front.

indicates that the gel is in tension. Ahead of this peel front, as indicated by the deformed region in Figure 5b, significant color change is observed that is highly position dependent and oscillates between longer and shorter wavelengths corresponding to both tensile and compressive regions of deformation.

Peel is similar to uniaxial deformation in that the stress or strain field can be described along a principle direction. The unique feature of peel is that the stress or strain field has a non-uniform distribution along this principle direction. This non-uniform distribution is attributed to local bending and stretching of the material, which can be described as a decaying sinusoidal function reflecting the alternating regions of tension and compression. For a 180° peel test, the stress distribution experienced by the gel as a function of the peel direction x is: $\sigma_z(x) = \sigma_0 \exp(-\beta x) (\cos \beta x + \sin \beta x)$, where $1/\beta$ is a characteristic length-scale that describes the gel region under tension or compression.^[64] To illustrate the effect of this stress distribution, we define the following stopband function vs. peel distance x by assuming that the photonic gel is a linear elastic material, whose mechanical response is also described by the junction-affine model, $(\alpha_z)^2 = (1 + (1 + \varepsilon_z)^2)/2$.^[63]

$$\lambda(x) = (2(n_{s,PS}d_{s,PS} + n_{s,PI}d_{s,PI})) \cdot \left(\frac{1 + (1 + \varepsilon_z)^2}{2} \right)^{1/2} \\ \approx (\lambda_0) \cdot \left(\frac{1 + (1 + e^{-\beta x} (\cos \beta x + \sin \beta x))^2}{2} \right)^{1/2} \quad (6)$$

Figure 5c is a plot of Equation 6 with $\lambda_0 = 2(n_{s,PS}d_{s,PS} + n_{s,PI}d_{s,PI}) = 500$ nm. The result demonstrates the effect of the peel stress

distribution on the local stopband shift: the stopband shifts to the highest wavelength at the peel front and then sinusoidally decays to λ_0 far away from the deformed region. One potential application of this photonic gel is thus in developing a better understanding of pressure sensitive adhesives. Here, the mechanochromic behavior would be quite useful as a visual sensor to detect failure or separation conditions of the an interface. These could be used for in situ monitoring; for example, the stopband shifting to longer wavelength will indicate that the adhesive is experiencing high stresses and is about to separate from a surface.

Plasticized BCP photonic gels can also be used to characterize shear. A polystyrene-*block*-poly(methyl methacrylate) (PS-*b*-PMMA) diblock copolymer ($M_{n,PS}/M_{n,PMMA} = 290\,000\text{ g mol}^{-1}/360\,000\text{ g mol}^{-1}$) was swollen with toluene^[65] (slight preference for the PS microdomain), and then sandwiched between two glass plates separated by a $150\ \mu\text{m}$ gap and strained at different linear strain rates (Figure 6). Interestingly, the mechanochromism of this photonic gel is strain-rate sensitive. At low strain rates (less than $\approx 0.1\text{ s}^{-1}$), the deformation produced

little change in the initial green color of the gel. Intermediate strain rates, however, produced a change in color from green to red with forward motion (away from the motor) and a slight blue-shift upon reversal. At higher strain rates (greater than $\approx 10\text{ s}^{-1}$), the sample changed from reflecting to transparent in appearance. One possible mechanism of this optical change is due to reorientation of the block copolymer microdomains along the shear direction. The gel regained color after several minutes following cessation of the shear deformation. This shear-rate-dependent behavior and slow recovery to the original undeformed state has also been recently reported by Mykhaylyk et al.,^[66] who probed the shear-induced morphological changes in a photonic BCP by using photo-crosslinking to lock in the transitory copolymer structures and enable traditional imaging techniques. Their results indicated that the strain-rate-dependent optical-property change is associated with reorientation of the lamellae from the parallel to the perpendicular orientation with increasing strain amplitude and rate.

Based on our previous discussion, a shift to longer wavelengths is due to an increase in the optical path length. With respect to shear, this change in optical path length is most likely due to an apparent increase of layer spacing caused by rotation of the microdomains as discussed previously (Figure 3c).^[67] Alternatively, the optical path length can increase due to a relative change in the refractive indices (e.g., cavitation of one of the microdomains due to deformation or enhanced swelling due to shear stress). However, this mechanism alone is insufficient to explain such a significant shift of the wavelength.

Further investigation on the microdomain structural changes with shear strain is required to understand the mechanism of stopband change completely. However, we can develop some

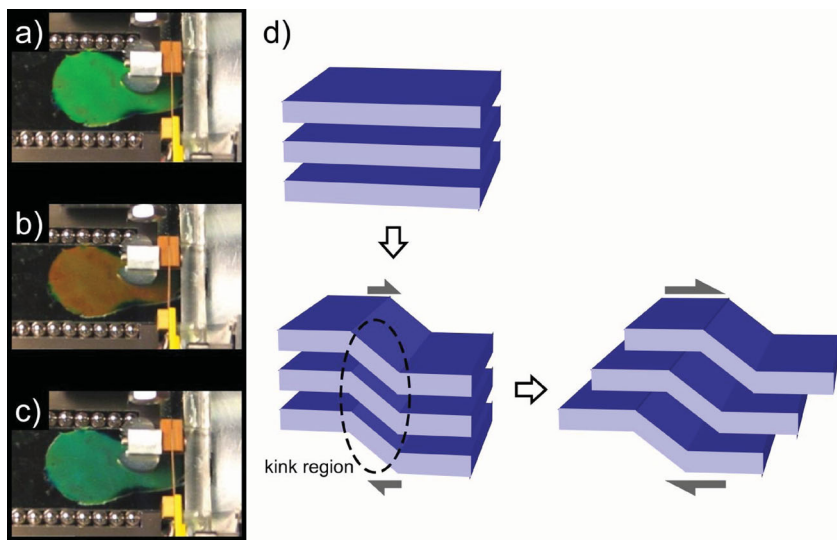


Figure 6. Simple shear of a PS-*b*-PMMA photonic gel. A cyclic shear (1 Hz) was applied to cause a transient color change of the photonic gel. A strain-rate of 3.3 s^{-1} produced a color change from green (a) to red (b) as viewed from above the gel. c) The reverse motion produced a slight blue-shift from the original sample color. d) Proposed microstructural evolution for the color change, which we suggest is associated with the formation of kinked microdomains at low shear and stretching of the kinked region with increasing shear.

qualitative understanding from previous work on the mechanical deformation of block copolymers. Specifically, researchers have shown that neat lamellar block copolymers have a tendency to form kink bands where regions of lamellae rotate under shear

normally oriented parallel with the substrate to perpendicular orientation or a significant breakup of the BCP structure leading to disorder. Upon cessation of shear, this clear state reverts back to the original stopband wavelength (i.e., the system goes from clear to green) after several minutes.

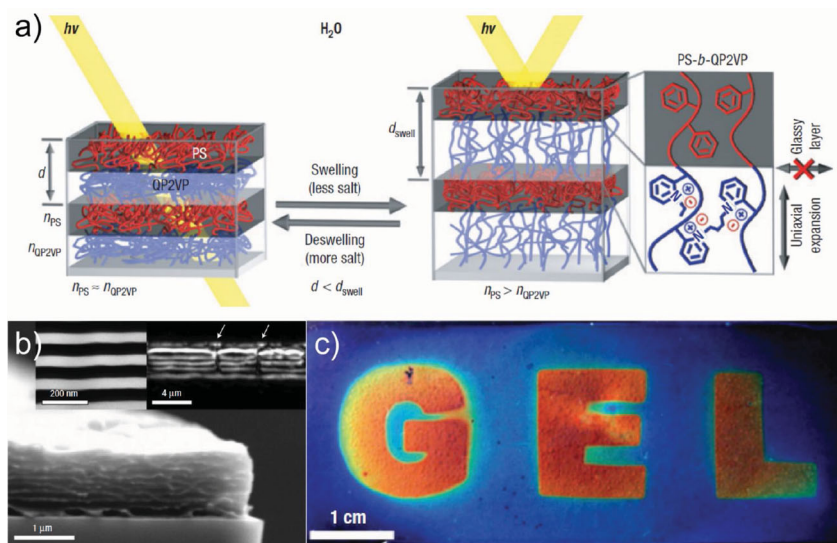


Figure 7. Optical properties of a polyelectrolyte PS-*b*-qP2VP photonic gel. a) Schematic of the BCP prior to swelling and the development of a photonic stopband following preferential swelling of the qP2VP microdomains with water. b) Three cross-sectional micrographs (transmission electron microscopy (TEM), confocal microscopy and scanning electron microscopy (SEM)) of the swollen gel at normal incidence, illustrating the microdomain structure. c) Optical micrograph of the photonic gel surface swollen in water. The red color of the letters GEL is due to the lower degree of crosslinking using dibromobutane compared with the blue background that swells less due to higher degree of crosslinking. Reproduced with permission.^[70] Copyright 2007, Nature Publishing Group.

deformation.^[67–69] Applying this deformation mechanism to the shearing photonic gel, a possible mechanism for stopband change is due to the formation of kink bands and stretching of the lamellae in the kinked regions. The material in the kinked region changes its domain spacing in response to the applied stress, whereas the material undergoes a rotation plus translation towards the shear direction as the polymer chains align with the flow direction. For example, when the strain rate is slow, the color remains constant because the system can relax faster than the shear can expand the material in the kinks. At intermediate strain rates, the chains cannot relax back to the preferred parallel orientation, which causes an expansion of the domains. The intensity of the red reflection also seems to decrease with an increasing number of cycles at these intermediate strain rates, suggesting that more and more chains could be aligning parallel to the shear direction with each successive cycle. At even higher strain rates, the system becomes clear due to an alignment of the chains parallel to the shear flow either due to the rotation of the lamellae that were originally oriented parallel with the substrate to perpendicular orientation or a significant breakup of the BCP structure leading to disorder. Upon cessation of shear, this clear state reverts back to the original stopband wavelength (i.e., the system goes from clear to green) after several minutes.

3.1.2. Polyelectrolyte BCP Photonic Gels

Incorporating a plasticizing agent provides a straightforward means to enhance the photonic properties of a diblock copolymer via uniform 3D swelling of both the block microdomains. However, preferential swelling of one of the blocks can be more effective in tailoring the intensity and peak wavelength of the stopband.

Kang et al. demonstrated this preferential large 1D swelling strategy using a polyelectrolyte BCP system.^[70] The starting BCP was a polystyrene-*block*-poly(2-vinylpyridine) (PS-*b*-P2VP) diblock copolymer ($M_{n,PS}/M_{n,P2VP} = 190\,000 \text{ g mol}^{-1}/190\,000 \text{ g mol}^{-1}$) that forms the lamellar morphology. Subsequent quaternization led to conversion of the P2VP microdomains into polyelectrolyte layers (qP2VP) that are stabilized after swelling by the adjacent glassy PS layers. This simple approach enabled the PS-*b*-qP2VP to develop chemical affinity to aqueous solutions. Exposure of this material to an electrolyte such as water caused selective and significant swelling (greater than $\approx 1000\%$) of the qP2VP microdomains, which resulted in the formation of a polyelectrolyte BCP photonic gel (Figure 7).

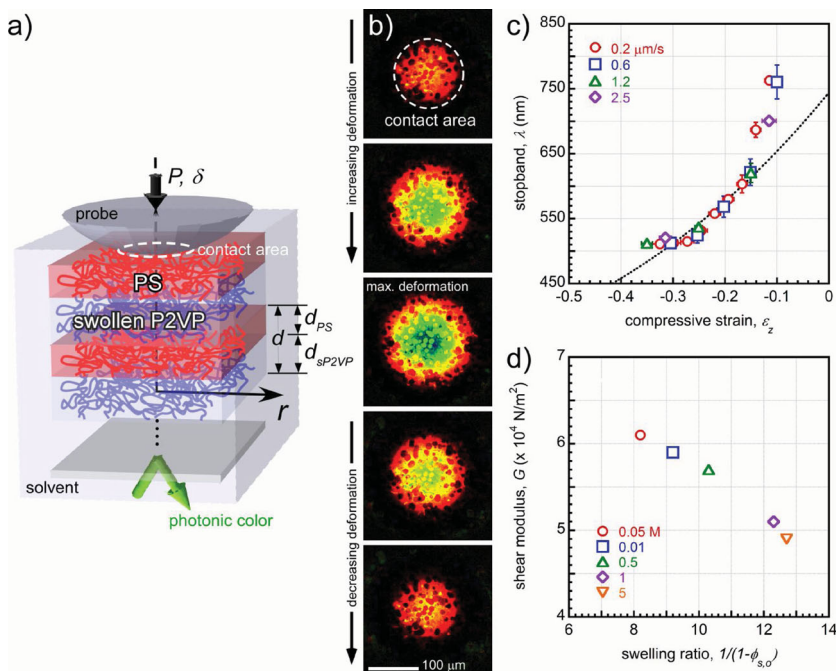


Figure 8. Mechanochromism of a polyelectrolyte PS-*b*-sP2VP photonic gel swollen with an acetic acid–water solution. a) Schematic of the deformation of the gel with a spherical probe with a glass probe of radius, $R = 5$ mm. b) Optical micrographs of the gel surface illustrating the change in stopband due to increasing compression by the probe. c) Stopband change versus compressive strain of the polyelectrolyte photonic gel for the central region. d) Tailoring the shear modulus with molar concentration of the acetic acid with respect to water, which leads to a corresponding change in the swelling ratio. Reproduced with permission.^[26] Copyright 2011, John Wiley & Sons, Inc.

This polyelectrolyte photonic gel system also displays mechanochromic behavior. Recently, Chan et al. demonstrated the mechanochromic response of a similar photonic gel via uniaxial compression testing (Figure 8).^[26] PS-*b*-P2VP diblock copolymer ($M_{n,S}/M_{n,P2VP} = 102\,000\text{ g mol}^{-1}/97\,000\text{ g mol}^{-1}$) was converted to a lamellar polyelectrolyte photonic gel upon exposure to an acetic acid–water solution that swells the P2VP domains by protonation. Contact mechanical testing was used to study the mechanochromic response. Specifically, the test involved deforming the gel under uniaxial compression and characterizing the applied compressive strain, stress, and contact area (Figure 8a). Due to the spherical shape of the indenter, an axisymmetric strain field developed within the region of the gel in contact, which is reflected by the radially dependent color observed in each normal-incidence light micrograph (Figure 8b). The indenter shape causes an increase in the contact area with increasing compressive strain (ϵ_z). Both these features are captured by the local color change of the photonic gel, which nicely demonstrated the ability of the BCP photonic gel to record localized mechanical deformation.

To describe the mechanochromic response, the position of the stopband measured at the center point of the contact area was measured as a function of compressive strain at several indentation rates (Figure 8c). A blue shift in the peak position with increasing compressive strain was observed while the stopband was insensitive to the indentation rates investigated.

The mechanochromic response is tunable with respect to the solution pH. The degree of swelling of the P2VP layers, and hence the average shear modulus of the photonic gel, changes significantly with the acetic acid concentration with respect to water (Figure 8d). This simple demonstration provided a straightforward means to adjust the mechanochromic sensitivity of the photonic gel, which enables a multitude of applications with different stress- or strain-detection requirements.

Additionally, Chan and co-workers developed a simple mechanical model, which considers the shift in the stopband to be associated purely with compression of the swollen P2VP (sP2VP) microdomains, with the PS microdomains acting as glassy layers stabilizing the overall structure.^[26] To improve upon their model, we develop a modified expression for stopband vs. strain. Similar to their model, we assume that this polyelectrolyte photonic gel is a linear elastic material with the sP2VP microdomain as the sole contributor to the total deformation. However, to relate the macroscopic deformation ratio to the local microdomain strain, we again apply the junction-affine model, $(\alpha_z)^2 = (1 + (1 + \epsilon_z)^2)/2$. Using the starting expression $\lambda = 2(n_{PS}d_{PS} + n_{sP2VP}d_{sP2VP})$ and then substituting the junction-affine model, we obtain:

$$\lambda(\epsilon_z) = 2(n_{PS}d_{PS} + n_{P2VP}d_{P2VP}) + 2n_s d_{P2VP} \left(\frac{(1 + (1 + \epsilon_z)^2)^{3/2}}{2} - 1 \right) \quad (7)$$

This model considers that compression causes deswelling of the sP2VP microdomains, with the macroscopic deformation ratio scaling with the swelling-agent volume fraction (ϕ_s) as $\alpha_z \approx ((1 - \phi_{s,0})/(1 - \phi_s))^{1/2}$ with the initial swelling ratio $(1 - \phi_{s,0})^{-1} \approx 10$. As shown in Figure 8c, Equation 7 is in fair agreement with the results, but fails to capture the invariance of the stopband at either the low or high compressive strains. We remark that Equation 7 predicts the stopband invariance, but at higher compressive strains than the experimental results, and the lack of agreement is attributed to several effects that this simple model does not account for. All of the microdomains are most likely not perfectly oriented parallel with the substrate, but consist of domains in other orientations that Equation 7 does not describe. Additionally, since the photonic gel is a highly swollen polymer network under mechanical constraint and deformation, interesting phenomena such as buckling instabilities can potentially occur. Buckling instabilities have been observed in many bilayer systems where one of the layers is a highly swollen polymer network.^[71–74] A similar phenomena may occur in these photonic gels where, in order to accommodate the significant expansion of the sP2VP layers, the

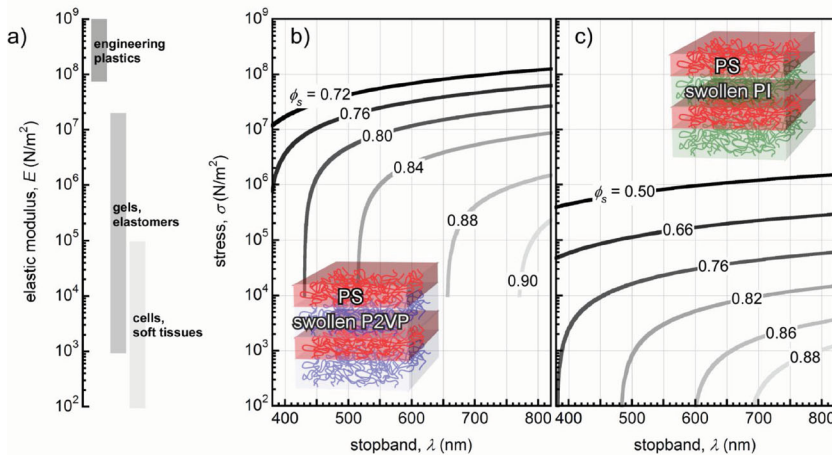


Figure 9. a) Elastic modulus range of several soft material classes. b) Prediction of the mechanochromism of a polyelectrolyte PS-*b*-sP2VP photonic gel as a function of acetic acid/water solution volume fraction. c) Prediction of the mechanochromism of a PS-*b*-sPI photonic gel as a function of tetradecane volume fraction.

PS layers buckle to maintain strain compatibility at the interfaces. At low strains, the deviation of the results compared with Equation 7 can potentially be attributed to poroelasticity. Poroelasticity is a field of physics that studies the coupling between the mass transport of a liquid within a porous medium. This phenomena has been observed in many polymers gels^[75–80] and will likely occur in photonic gels since the mechanochromism of these materials is associated with solvent migration within the gel due to mechanical deformation. Since the poroelastic relaxation time scales with the diffusion length squared over the diffusion constant $\approx a^2/D$, this implies that there is a finite time requirement for solvent migration, and thus the stopband shift with strain is time-dependent. At low strains or initial testing times, the poroelastic relaxation time can be longer than the testing time, thus implying that the solvent concentration is higher than predicted by Equation 7. Therefore, future work warrants morphological characterization of the microdomains with emphasis on establishing relationships to quantify the expansion ratio of the microdomain layers vs. solvent volume fraction; the change in solvent volume fraction vs. compressive strain and time; and the compressive strain vs. microdomain layer thicknesses and time.

3.1.3. Tuning the Mechanochromic Response of BCP Photonic Gels

The broad application of these photonic gels as mechanochromic sensors requires that they can mechanically couple to the material of interest and report the local strain field. In other words, the photonic gel must have similar mechanical properties to the material of interest. With soft materials, their elastic modulus can span from approximately 10² N m⁻² for cells and soft tissues up to approximately 10⁹ N m⁻² for engineering plastics (Figure 9a). For a photonic gel to serve as a functional sensor over this entire range requires manipulating its moduli by 7 orders of magnitude.

While this presents a significant material requirement, BCP photonic gels offer many opportunities for tuning the

optical and mechanical properties via the incorporation of the appropriate swelling agents. Figure 9b and 9c illustrate 2 possible approaches. These figures are predictions of the mechanochromic behavior for PS-*b*-P2VP swollen with acetic acid (PS-*b*-sP2VP)^[26,81] and PS-*b*-PI swollen with tetradecane (PS-*b*-sPI),^[82] two systems that have been experimentally demonstrated as block copolymer gels that undergo preferential swelling. In both examples, the starting block copolymers are symmetric diblocks that form the lamellar morphology. Next, a specific preferential solvent is added to swell one of the blocks to form the photonic gel, which leads to an increase in the domain spacing and a decrease in the refractive index of the swollen block. To predict the stopband change due to an applied compressive stress normal to the microdomain layers, we assume that the photonic gel is linear elastic. For PS-*b*-sP2VP, the stress vs. strain relationships for the two

blocks are: $\sigma_{PS} = E_{PS}\epsilon_{PS}$ and $\sigma_{sP2VP} = E_{sP2VP}\epsilon_{sP2VP}$, where E_{PS} and E_{sP2VP} are the elastic moduli of the PS and sP2VP layers, respectively. Again, we apply the Reuss model to describe the mechanical response of the photonic gel, the total stress $\sigma_z = \sigma_{PS} = \sigma_{sP2VP}$. Substitution of these expressions into Equation 1 yields:

$$\lambda(\sigma_z) = 2n_{PS}d_{PS} \left(1 + \frac{\sigma_z}{E_{PS}}\right) + 2n_{sP2VP}d_{sP2VP} \left(1 + \frac{\sigma_z}{E_{sP2VP}}\right) \quad (8)$$

The elastic modulus of the PS layer (E_{PS}) is a constant. The elastic modulus of the sP2VP changes with volume fraction of the acetic acid (ϕ_s), $E_{sP2VP} \approx E_{P2VP}(1 - \phi_s)^3$, where we consider the sP2VP as a gel swollen with an uncharged solvent.^[83] Substituting these expressions into Equation 8, along with the relationships of refractive index $n_{sP2VP} = \phi_s n_s + (1 - \phi_s)n_{P2VP}$ and domain spacing ($d_{sP2VP} = d_{P2VP}/(1 - \phi_s)$) of the sP2VP, we obtain:

$$\lambda(\sigma_z) = 2(n_{PS}d_{PS} + n_{P2VP}d_{P2VP}) + 2n_s d_{P2VP} \cdot \left(\frac{1}{\phi_s} - 1\right)^{-1} + 2\sigma_z \cdot \left(\frac{n_{PS}d_{PS}}{E_{PS}} + \frac{n_{P2VP}d_{P2VP}}{E_{P2VP}}(1 - \phi_s)^{-3} + \frac{n_s d_{P2VP}}{E_{P2VP}} \phi_s (1 - \phi_s)^{-4}\right) \quad (9)$$

Using the materials constants ($E_{PS} \approx E_{P2VP} \approx 3 \times 10^9$ N m⁻², $n_{PS} = 1.59$, $n_{P2VP} = 1.62$, $n_s = 1.35$) into Equation 9 yields the results in Figure 9b for several acetic acid volume fractions. We also use Equation 9 to predict the mechanochromic response of

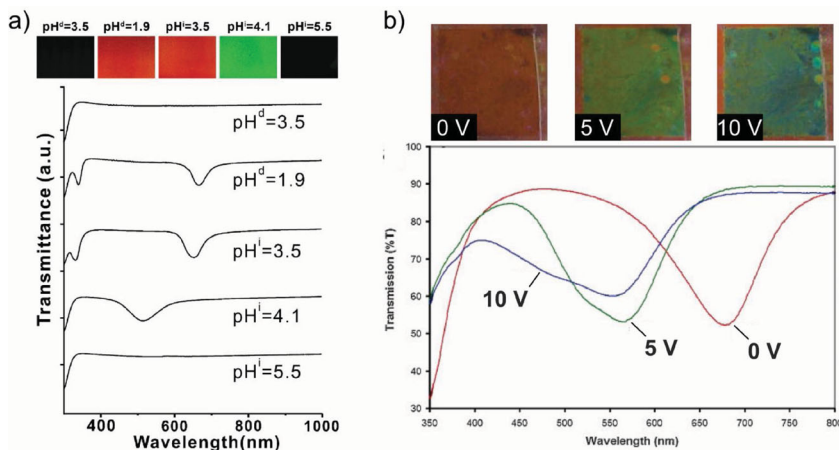


Figure 10. Examples of stimuli-responsive PS-*b*-qP2VP photonic gels. The stopband can be controlled via changes in: a) pH and b) electrochemical potential. a) Reproduced with permission.^[81] Copyright 2010, John Wiley & Sons, Inc. b) Reproduced with permission.^[84] Copyright 2009, John Wiley & Sons, Inc.

the PS-*b*-sPI by substituting the materials constants of sP2VP with sPI ($E_{PI} \approx 3 \times 10^6 \text{ N m}^{-2}$, $n_{PI} = 1.52$, $n_{PI} = 1.43$), and the results are summarized in Figure 9c at several tetradecane volume fractions.

The relationship of stress to stopband position depicted in Figure 9b and Figure 9c illustrates the general strategy to obtaining a BCP photonic gel with a highly tunable mechanochromic response, that is, a material platform that can measure a large range of stresses via observation of a photonic stopband in the visible wavelength regime. Based on these results, the range of measurable stress of the photonic gel is determined primarily by the block with the lower modulus. The upper limit of the stress range is determined by the modulus of the dry block and the lower limit of the stress range is determined at the maximum solvent volume fraction. Comparing the two photonic gels, the PS-*b*-sPI system is predicted to be able to measure lower stresses than the PS-*b*-sP2VP system at similar solvent volume fractions. This result is attributed to the lower modulus of the starting rubbery PI block compared with the glassy P2VP block. Preferential swelling leads to a decrease in the moduli of the respective blocks and an enhanced sensitivity to lower levels of stress. However, significant swelling can potentially render the photonic gel as a non-functioning mechanochromic sensor because the primary stopband will be outside the visible region.

The PS-*b*-P2VP BCP is a highly tunable photonic gel platform since the pyridine group of the P2VP block is responsive to various stimuli, such as pH or electric field. For example, Kim et al. demonstrated that the stopband of the PS-*b*-qP2VP photonic gel can be tuned via changes in pH (Figure 10a).^[81] This pH-dependent swelling behavior is related to the qP2VP ion-pairing affinity between the protonated pyridinium on the qP2VP and the various anions of the buffered solution. Therefore, the stopband can be tuned simply by the addition of an acid or base to control the ion-pairing affinity.

Alternatively, the stopband can be tuned electrochemically. Walsh et al. presented a simple full-color pixel device based on

a similar PS-*b*-sP2VP photonic gel swollen with 2,2,2-trifluoroethanol (Figure 10b).^[84] Upon application of an electric field, this electrolytic swelling agent can undergo a redox reaction that leads to dissociation into trifluoroethoxide ions. This dissociation effectively changes the solvent quality, which leads to deswelling of the sP2VP domains and a shift of the stopband to shorter wavelengths.

3.2. Colloidal Crystal Photonic Gels

3.2.1. Spherical Colloidal Crystal Photonic Gels

Gel-immobilized colloidal crystals represent the most common type of 3D mechanochromic photonic gel (Figure 11). Generally, this composite gel consists of a close-packed array of colloidal particles, such as polymeric or inorganic microspheres, which is infiltrated with or encapsulated by a crosslinked polymer gel (Figure 11a). Thus, these gels share similarities with BCP photonic gels in that they are composites of two components with different mechanical properties. As there are many approaches to fabricating such gel-immobilized colloidal crystals, please refer to refs.^[13,18,19,27,85–87]

The advantage in using a 3D photonic crystal is that it offers the possibility of a complete photonic bandgap, provided that there is sufficient dielectric contrast and the proper 3D structure. A 3D crystal allows for mechanochromic sensing in all three directions. However, current 3D photonic gels have been limited to mechanochromic sensing along a single principal

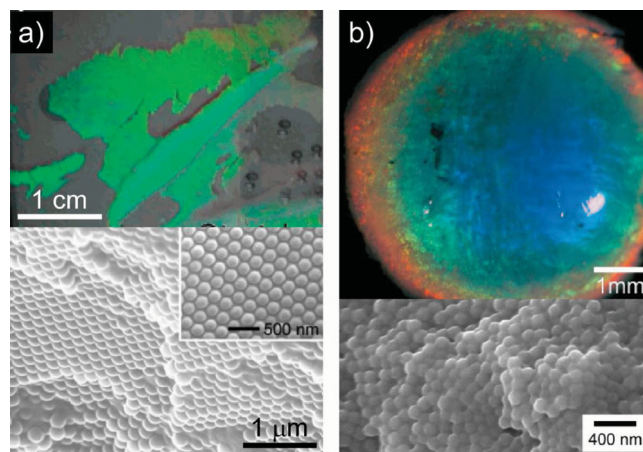


Figure 11. Examples of 3D photonic structures. a) 3D photonic elastomer based on infiltration of close-packed PS spheres with an elastomeric precursor followed by crosslinking. Reproduced with permission.^[18] Copyright 2005, The American Chemical Society. b) 3D photonic gel based on centrifugation of *Wisena* iridovirus and subsequent crosslinking of the pellet. Reproduced with permission.^[88] Copyright 2006, John Wiley & Sons, Inc.

direction.^[11–14,18,20,22] In other words, these 3D photonic gels are utilized as mechanochromic sensors in the same way as the 1D photonic gels discussed earlier, and their utility as 3D sensors has yet to be realized. Under uniaxial compression or tension, the mechanochromic response of these 3D photonic gels is associated with the change in spacing of close-packed planes defined by the colloidal crystal assembly.^[11–14] Thus, the stopband shift with stress and strain is related in a fairly straightforward manner. Similar to the 1D photonic gels, these 3D photonic gels have been demonstrated as simple pressure sensors.^[11–14,18–21] Again, the range of stresses that can be measured by these gels is dependent on the moduli of the gel matrices, which typically have been on the order of $\approx 10^4$ to 10^5 N m⁻².

3.2.2. Iridovirus Photonic Gels

An alternative to the gel-infiltrated colloidal crystal photonic gel is the iridovirus-based photonic gel. Iridoviruses, a name originally derived because of the “rainbow-like” iridescence observed in heavily infected insects, are nanoparticles with an icosahedral shape. Compared with the synthetic spherical particles typically used in 3D photonic crystals, iridoviruses are unique for their non-spherical-like shapes with monodisperse particle dimensions and highly defined surface chemistries. These virus particles are potentially interesting material platforms for assembling 3D photonic crystals with symmetries different from the traditional structures obtained using spherical particles.

Iridoviruses have been observed to form 3D photonic crystals in vivo and, more recently, in vitro. Previously, Juhl et al. demonstrated that either centrifugation or flow-assisted assembly can be used to generate a 3D photonic gel of chemically crosslinked *Wiseana* iridescent virus (WIV) particles (Figure 11b).^[88] The researchers showed that the morphology of the WIV assembly depended on the processing method. Centrifugation yielded disordered but densely packed structure with short-range order, whereas flow-assistance assembly yielded a close-packed polycrystalline structure. Following processing, the morphology of the WIV structure can be locked in by taking advantage of the surface chemistry of the WIV via chemical crosslinking with glutaraldehyde to form the iridovirus photonic gel. The interesting result is that both processing methods yield WIV assemblies with photonic properties that can be reversibly tuned via swelling. While the mechanical properties of these virus assemblies are not known, their reversible swelling behavior suggests their potential as mechanochromic photonic gel sensors.

One final point is the importance of long-range order on the photonic properties of these gels. Traditionally, photonic crystals are commonly associated with materials having long-range order, resulting in Bragg scattering. Therefore, defects or disorder in a photonic crystal were considered undesirable, as they are assumed to lead to a decrease in optical properties. However, recent simulation and experimental work have demonstrated that disordered materials such as colloidal glasses can develop photonic bandgaps.^[89–92] Using both theory and numerical simulations, Florescu et al. suggest that the three materials requirements for obtaining a photonic crystal with a complete bandgap include hyperuniformity, uniform local

topology, and short-range geometric order, which are automatically satisfied by both photonic crystals and quasicrystals.^[92] These requirements also exist in some colloidal glasses that are hyperuniform, that is to say, density fluctuations are minimized over large length scales. Therefore, designing colloidal glasses as photonic bandgap materials would require computations and modeling to identify glass structures that satisfy the three materials requirements necessary for a complete bandgap. Compared with the traditional 3D photonic gels that require colloidal crystal templates with long-range order, these results may have a significant impact from a fabrication standpoint, since they suggest a more pragmatic approach to generating photonic gels based on colloidal glasses without the need to achieve long-range order with minimal defects.

4. Conclusions and Future Outlook

In this report, we have shown several examples of structured polymer-based materials that exhibit strain-dependent photonic properties. These mechanochromic materials have potential applications in sensing, monitoring and revealing complex local strain fields that can be quantified provided that the exact relationships between the stopband and the strain or stress are established. While the development of these materials is ongoing, we have shown that simple relationships linking the structures, their mechanical properties, optical properties, and mechanochromic response can be derived to describe experimental results. These can serve as an enabling starting point to this field as it develops. Clearly, complex phenomena remain to be explained and new materials systems developed to exploit mechanochromism fully. Key hurdles include the analysis of complex strains in heterogeneous systems and dynamic responses (time-dependent phenomena such as polymer viscoelasticity and poroelasticity), increasing the response of materials systems, and generating a wider range of available mechanical properties for visible mechanochromic materials. In particular, experimental measurements that can quantify local changes to the structure (microdomain reorientation) and composition (solvent/polymer distribution) are needed. Measurement tools such as X-ray scattering^[93,68,67] and neutron scattering,^[63] coupled with in situ mechanical deformation of the photonic gels is especially useful in providing quantitative information with regard to changes in structure and composition. However, these measurement tools are best suited for quasi-static experiments because of their relatively slow data-acquisition times. Alternatively, advanced imaging techniques such as stimulated emission depletion microscopy^[94,95] and laser scanning confocal microscopy^[96] potentially provide the fast acquisition times needed for capturing the rapid changes in structure and composition due to in situ mechanical testing. While these imaging techniques have been demonstrated for imaging the nanostructures of high-molecular-mass BCPs, they may still lack the resolution needed to quantify the compositional changes due to mechanical deformation. Thus, future studies in linking mechanochromism to local structural and compositional changes of structured polymer-based materials may involve utilizing both scattering and advanced imaging techniques in order to obtain the necessary material information.

Acknowledgements

E.L.T. acknowledges the Air Force Office of Scientific Research (AOARD R&D Grant 114078 & Grant 114095), and the Defense Threat Reduction Agency (HDTA1-12-1-0044) for financial support. Official contribution of the National Institute of Standards and Technology; not subject to copyright in the United States. Certain commercial equipment, instruments, or materials are identified in this paper in order to specify the experimental procedure adequately. Such identification is not intended to imply recommendation or endorsement by the National Institute of Standards and Technology, nor is it intended to imply that the materials or equipment identified are necessarily the best available for the purpose.

Received: February 11, 2013

Revised: April 1, 2013

Published online:

- [1] S. Kinoshita, S. Yoshioka, *ChemPhysChem* **2005**, *6*, 1442–1459.
- [2] S. Kinoshita, S. Yoshioka, J. Miyazaki, *Rep. Prog. Phys.* **2008**, *71*, 076401.
- [3] A. R. Parker, *J. Opt. A: Pure Appl. Opt.* **2000**, *2*, R15.
- [4] Y. Fink, J. N. Winn, S. Fan, C. Chen, J. Michel, J. D. Joannopoulos, E. L. Thomas, *Science* **1998**, *282*, 1679–1682.
- [5] S. D. Hart, G. R. Maskaly, B. Temelkuran, P. H. Prideaux, J. D. Joannopoulos, Y. Fink, *Science* **2002**, *296*, 510–513.
- [6] J. Yoon, W. Lee, J.-M. Caruge, M. Bawendi, E. L. Thomas, S. Kooi, P. N. Prasad, *Appl. Phys. Lett.* **2006**, *88*, 091102.
- [7] M. Ben-Moshe, V. L. Alexeev, S. A. Asher, *Anal. Chem.* **2006**, *78*, 5149–5157.
- [8] S. Asher, S. Peteu, C. Reese, M. Lin, D. Finegold, *Anal. Bioanal. Chem.* **2002**, *373*, 632–638.
- [9] Y.-J. Lee, P. V. Braun, *Adv. Mater.* **2003**, *15*, 563–566.
- [10] W. Hong, X. Hu, B. Zhao, F. Zhang, D. Zhang, *Adv. Mater.* **2010**, *22*, 5043–5047.
- [11] S. A. Asher, J. Holtz, L. Liu, Z. Wu, *J. Am. Chem. Soc.* **1994**, *116*, 4997–4998.
- [12] J. M. Jethmalani, W. T. Ford, *Chem. Mater.* **1996**, *8*, 2138–2146.
- [13] S. H. Foulger, P. Jiang, A. C. Lattam, Smith, J. Ballato, *Langmuir* **2001**, *17*, 6023–6026.
- [14] S. H. Foulger, P. Jiang, Y. Ying, A. C. Lattam, D. W. Smith Jr., J. Ballato, *Adv. Mater.* **2001**, *13*, 1898–1901.
- [15] H. Finkelmann, S. T. Kim, A. Muñoz, P. Palffy-Muhoray, B. Taheri, *Adv. Mater.* **2001**, *13*, 1069–1072.
- [16] S. H. Foulger, P. Jiang, A. Lattam, D. Smith Jr., J. Ballato, D. E. Dausch, S. Grego, B. R. Stoner, *Adv. Mater.* **2003**, *15*, 685–689.
- [17] S. A. Holmstrom, L. V. Natarajan, V. P. Tondiglia, R. L. Sutherland, T. J. Bunning, *Appl. Phys. Lett.* **2004**, *85*, 1949.
- [18] H. Fudouzi, T. Sawada, *Langmuir* **2005**, *22*, 1365–1368.
- [19] A. C. Arsenault, T. J. Clark, G. von Freymann, L. Cademartiri, R. Sapienza, J. Bertolotti, E. Vekris, S. Wong, V. Kitaev, I. Manners, R. Z. Wang, S. John, D. Wiersma, G. A. Ozin, *Nat. Mater.* **2006**, *5*, 179–184.
- [20] Y. Ying, J. Xia, S. H. Foulger, *Appl. Phys. Lett.* **2007**, *90*, 071110.
- [21] B. Viel, T. Ruhl, G. P. Hellmann, *Chem. Mater.* **2007**, *19*, 5673–5679.
- [22] Y. Ying, S. H. Foulger, *Sensors Actuators B* **2009**, *137*, 574–577.
- [23] M. A. Haque, G. Kamita, T. Kurokawa, K. Tsujii, J. P. Gong, *Adv. Mater.* **2010**, *22*, 5110–5114.
- [24] D. K. Cullen, Y. Xu, D. V. Reneer, K. D. Browne, J. W. Geddes, S. Yang, D. H. Smith, *NeuroImage* **2011**, *54*, Supplement 1, S37–S44.
- [25] L. M. Fortes, M. C. Gonçalves, R. M. Almeida, *Opt. Mater.* **2011**, *33*, 408–412.
- [26] E. P. Chan, J. J. Walsh, E. L. Thomas, C. M. Stafford, *Adv. Mater.* **2011**, *23*, 4702–4706.
- [27] A. C. Arsenault, D. P. Puzzo, I. Manners, G. A. Ozin, *Nat. Photonics* **2007**, *1*, 468–472.
- [28] K. Hwang, D. Kwak, C. Kang, D. Kim, Y. Ahn, Y. Kang, *Angew. Chem., Int. Ed.* **2011**, *50*, 6311–6314.
- [29] Y. Lu, H. Xia, G. Zhang, C. Wu, *J. Mater. Chem.* **2009**, *19*, 5952.
- [30] M. Ibanescu, Y. Fink, S. Fan, E. L. Thomas, J. D. Joannopoulos, *Science* **2000**, *289*, 415–419.
- [31] B. Temelkuran, S. D. Hart, G. Benoit, J. D. Joannopoulos, Y. Fink, *Nature* **2002**, *420*, 650–653.
- [32] R. W. Ryan, T. Wolf, R. F. Spetzler, S. W. Coons, Y. Fink, M. C. Preul, *J. Neurosurgery* **2010**, *112*, 434–443.
- [33] J. D. Joannopoulos, *Photonic Crystals: Molding The Flow Of Light*, Princeton University Press, NJ, USA **2008**.
- [34] W. J. Schrenk, W. E. Shrum, J. A. Wheatley, US Patent 4937134, **1990**.
- [35] T. Kazmierczak, H. Song, A. Hiltner, E. Baer, *Macromol. Rapid Commun.* **2007**, *28*, 2210–2216.
- [36] M. Kolle, A. Lethbridge, M. Kreysing, J. J. Baumberg, J. Aizenberg, P. Vukusic, *Adv. Mater.* **2013**, *25*, 2239–2245.
- [37] S. A. Holmstrom, L. V. Natarajan, V. P. Tondiglia, R. L. Sutherland, T. J. Bunning, *Appl. Phys. Lett.* **2004**, *85*, 1949–1951.
- [38] M. A. Haque, T. Kurokawa, G. Kamita, J. P. Gong, *Macromolecules* **2011**, *44*, 8916–8924.
- [39] M. J. Cromie, *M.S. Thesis*, Massachusetts Institute of Technology, Boston, MA USA **2005**.
- [40] J. Yoon, *Ph.D. Thesis*, Massachusetts Institute of Technology, Boston, MA USA **2006**.
- [41] T. Alfrey Jr., E. F. Gurnee, W. J. Schrenk, *Polymer Engineering & Science* **1969**, *9*, 400–404.
- [42] C. D. Mueller, S. Nazarenko, T. Ebeling, T. L. Schuman, A. Hiltner, E. Baer, *Polym. Eng. Sci.* **1997**, *37*, 355–362.
- [43] T. J. Hebrink, Y. J. Liu, W. W. Merrill, B. A. Nerad, J. A. Wheatley, US Patent 6830713, **2004**.
- [44] M. F. Weber, C. A. Stover, L. R. Gilbert, T. J. Nevitt, A. J. Ouder Kirk, *Science* **2000**, *287*, 2451–2456.
- [45] J. W. Mays, N. Hadjichristidis, L. J. Fetters, *Macromolecules* **1985**, *18*, 2231–2236.
- [46] Y. Fink, A. M. Urbas, M. G. Bawendi, J. D. Joannopoulos, E. L. Thomas, *J. Lightwave Technol.* **1999**, *17*, 1963–1969.
- [47] A. C. Edrington, A. M. Urbas, P. DeRege, C. X. Chen, T. M. Swager, N. Hadjichristidis, M. Xenidou, L. J. Fetters, J. D. Joannopoulos, Y. Fink, E. L. Thomas, *Adv. Mater.* **2001**, *13*, 421–425.
- [48] S. B. Darling, *Prog. Polym. Sci.* **2007**, *32*, 1152–1204.
- [49] C.-Y. Chao, X. Li, C. K. Ober, C. Osuji, E. L. Thomas, *Adv. Funct. Mater.* **2004**, *14*, 364–370.
- [50] C. Osuji, C.-Y. Chao, I. Bitá, C. K. Ober, E. L. Thomas, *Adv. Funct. Mater.* **2002**, *12*, 753–758.
- [51] M. Mitov, E. Nouvet, N. Dessaud, *Eur. Phys. J. E* **2004**, *15*, 413–419.
- [52] J.-Y. Chen, L.-W. Chen, *Phys. B: Condensed Matter* **2005**, *357*, 282–289.
- [53] M. Warner, E. M. Terentjev, R. B. Meyer, Y. Mao, *Phys. Rev. Lett.* **2000**, *85*, 2320–2323.
- [54] P. A. Bermel, M. Warner, *Phys. Rev. E* **2001**, *65*, 010702.
- [55] R. Zentel, G. Reckert, *Makromol. Chem.* **1986**, *187*, 1915–1926.
- [56] A. Arsenault, V. Kitaev, I. Manners, G. Ozin, A. Mihi, H. Miguez, *J. Mater. Chem.* **2005**, *15*, 133–138.
- [57] J. R. Lawrence, G. H. Shim, P. Jiang, M. G. Han, Y. Ying, S. H. Foulger, *Adv. Mater.* **2005**, *17*, 2344–2349.
- [58] J. R. Lawrence, Y. Ying, P. Jiang, S. H. Foulger, *Adv. Mater.* **2006**, *18*, 300–303.
- [59] A. M. Urbas, M. Maldovan, P. DeRege, E. L. Thomas, *Adv. Mater.* **2002**, *14*, 1850–1853.
- [60] A. Urbas, R. Sharp, Y. Fink, E. L. Thomas, M. Xenidou, L. J. Fetters, *Adv. Mater.* **2000**, *12*, 812–814.

- [61] M. Bockstaller, R. Kolb, E. L. Thomas, *Adv. Mater.* **2001**, *13*, 1783–1786.
- [62] A. M. Urbas, *Ph.D. Thesis*, Massachusetts Institute of Technology, Boston, MA USA **2003**.
- [63] T. Matsunaga, H. Asai, Y. Akagi, T. Sakai, U. Chung, M. Shibayama, *Macromolecules* **2011**, *44*, 1203–1210.
- [64] D. H. Kaelble, *J. Colloid Sci.* **1964**, *19*, 413–424.
- [65] J. J. Walish, *Ph.D. Thesis*, Massachusetts Institute of Technology, Boston, MA USA **2008**.
- [66] O. O. Mykhaylyk, A. J. Parnell, A. Pryke, J. P. A. Fairclough, *Macromolecules* **2012**, *45*, 5260–5272.
- [67] Y. Cohen, R. J. Albalak, B. J. Dair, M. S. Capel, E. L. Thomas, *Macromolecules* **2000**, *33*, 6502–6516.
- [68] D. L. Polis, S. D. Smith, N. J. Terrill, A. J. Ryan, D. C. Morse, K. I. Winey, *Macromolecules* **1999**, *32*, 4668–4676.
- [69] L. Qiao, K. I. Winey, *Macromolecules* **2000**, *33*, 851–856.
- [70] Y. Kang, J. J. Walish, T. Gorishnyy, E. L. Thomas, *Nat. Mater.* **2007**, *6*, 957–960.
- [71] E. A. Wilder, S. Guo, S. Lin-Gibson, M. J. Fasolka, C. M. Stafford, *Macromolecules* **2006**, *39*, 4138–4143.
- [72] E. P. Chan, A. J. Crosby, *Soft Matter* **2006**, *2*, 324–328.
- [73] J. Y. Chung, A. J. Nolte, C. M. Stafford, *Adv. Mater.* **2009**, *21*, 1358–1362.
- [74] E. P. Chan, A. J. Crosby, *Adv. Mater.* **2006**, *18*, 3238–3242.
- [75] M. Doi, *J. Phys. Soc. Jpn.* **2009**, *78*, 052001.
- [76] Y. Hu, X. Zhao, J. J. Vlassak, Z. Suo, *Appl. Phys. Lett.* **2010**, *96*, 121904.
- [77] X. Zhao, N. Huebsch, D. J. Mooney, Z. Suo, *J. Appl. Phys.* **2010**, *107*, 063509.
- [78] Y. Hu, X. Chen, G. M. Whitesides, J. J. Vlassak, Z. Suo, *J. Mater. Res.* **2011**, *26*, 785–795.
- [79] Y. Hu, E. P. Chan, J. J. Vlassak, Z. Suo, *J. Appl. Phys.* **2011**, *110*, 086103.
- [80] E. P. Chan, Y. Hu, P. M. Johnson, Z. Suo, C. M. Stafford, *Soft Matter* **2012**, *8*, 1492–1498.
- [81] E. Kim, C. Kang, H. Baek, K. Hwang, D. Kwak, E. Lee, Y. Kang, E. L. Thomas, *Adv. Funct. Mater.* **2010**, *20*, 1728–1732.
- [82] K. J. Hanley, T. P. Lodge, C.-I. Huang, *Macromolecules* **2000**, *33*, 5918–5931.
- [83] S. P. Obukhov, M. Rubinstein, R. H. Colby, *Macromolecules* **1994**, *27*, 3191–3198.
- [84] J. J. Walish, Y. Kang, R. A. Mickiewicz, E. L. Thomas, *Adv. Mater.* **2009**, *21*, 3078–3081.
- [85] K. Lee, S. Asher, *J. Am. Chem. Soc.* **2000**, *122*, 9534–9537.
- [86] C. Chen, Y. Zhu, H. Bao, P. Zhao, H. Jiang, L. Peng, X. Yang, C. Li, *Soft Matter* **2010**, *7*, 915–921.
- [87] J. Wang, Y. Han, *J. Colloid Interface Sci.* **2011**, *353*, 498–505.
- [88] S. B. Juhl, E. P. Chan, Y.-H. Ha, M. Maldovan, J. Brunton, V. Ward, T. Dokland, J. Kalmakoff, B. Farmer, E. L. Thomas, R. A. Vaia, *Adv. Funct. Mater.* **2006**, *16*, 1086–1094.
- [89] P. D. García, R. Sapienza, Á. Blanco, C. López, *Adv. Mater.* **2007**, *19*, 2597–2602.
- [90] I. Lee, D. Kim, J. Kal, H. Baek, D. Kwak, D. Go, E. Kim, C. Kang, J. Chung, Y. Jang, S. Ji, J. Joo, Y. Kang, *Adv. Mater.* **2010**, *22*, 4973–4977.
- [91] Z.-Y. Li, Z.-Q. Zhang, *Phys. Rev. B* **2000**, *62*, 1516–1519.
- [92] M. Florescu, S. Torquato, P. J. Steinhardt, *Proc. Natl. Acad. Sci. USA* **2009**, *106*, 20658–20663.
- [93] C. C. Honeker, E. L. Thomas, *Chem. Mater.* **1996**, *8*, 1702–1714.
- [94] C. K. Ullal, R. Schmidt, S. W. Hell, A. Egner, *Nano Lett.* **2009**, *9*, 2497–2500.
- [95] C. K. Ullal, S. Primpke, R. Schmidt, U. Böhm, A. Egner, P. Vana, S. W. Hell, *Macromolecules* **2011**, *44*, 7508–7510.
- [96] J. Yoon, W. Lee, E. L. Thomas, *Adv. Mater.* **2006**, *18*, 2691–2694.